Available online at www.sciencedirect.com
ScienceDirect
Journal of the European Ceramic Society 27 (2007) 4489–4497
www.elsevier.com/locate/jeurceramsoc

Formation of $BaTiO_3$ nanoparticles from an aqueous precursor by flame-assisted spray pyrolysis

Agus Purwanto [a], Wei-Ning Wang [a], I. Wuled Lenggoro [b], Kikuo Okuyama [a,*]

[a] *Department of Chemical Engineering, Graduate School of Engineering, Hiroshima University, 1-4-1 Kagamiyama, Higashi Hiroshima, Hiroshima 739-8527, Japan*
[b] *Institute of Symbiotic Science and Technology, Tokyo University of Agriculture and Technology, 2-24-16 Naka-cho, Koganei, Tokyo 184-8588, Japan*

Received 14 December 2006; received in revised form 3 April 2007; accepted 14 April 2007
Available online 18 June 2007

Abstract

By manipulating process parameters, $BaTiO_3$ nanoparticles with tunable size were successfully prepared by flame-assisted spray pyrolysis (FASP) from an aqueous solution of barium acetate and titanium-tetra-isopropoxite. Particle size was controlled over a wide range (from about 23 to 71 nm) by varying the concentration of precursor and methane flow rate. Flame temperature was a key factor in producing particles with a narrow size distribution. The $BaTiO_3$ nanoparticles were cubic in crystal structure, dense, spherical and softly agglomerated. The particles contained OH, carboxyl and CO_2 bonding groups that could be completely removed by post-heat treatment. At room temperature, $BaTiO_3$ pellets had relatively high dielectric constants (2578.8–3611.8) with loss factors ranging from 2.6% to 7.1% at the frequency of 1 kHz. The results of this study indicate that $BaTiO_3$ nanoparticles can be fabricated using continuous and industrially applicable FASP.

Keywords: Aerosol; Dielectric properties; Impedance; $BaTiO_3$ and titanates; Capacitors

1. Introduction

$BaTiO_3$ is one of the most widely used materials in the electro-ceramics industry. It is used in multilayer ceramic capacitors (MLCCs), thermistors, electro-optic devices and dynamic random-access ferroelectric memories (DRAMs).[1–3] $BaTiO_3$ has a perovskite structure, possesses a high dielectric constant, is chemically stable and has tunable physical properties.[2] In the last decade, the size of electronic devices has been scaled down, driving the development of smaller electronic components. To meet this requirement, fabrication of very fine $BaTiO_3$ particles with good electrical properties is necessary.

The conventional method of preparing $BaTiO_3$ particles is via a solid-state reaction from the calcinations of $BaCO_3$ and TiO_2.[4–8] The as-prepared powder is typically coarse and highly agglomerated. Recently, $BaTiO_3$ nanoparticles have been prepared via this method from nanocrystalline TiO_2.[5] However, this method is time-consuming and energy-intensive. Hydrothermal,[4,9,10] sol–gel,[11,12] precipitation,[3,13] and combustion[14] methods also can be used to prepare ultrafine $BaTiO_3$ particles. As batch processes, liquid-phase methods are quite simple; however, the likelihood of producing an impure product is high. Therefore, products produced using liquid-phase methods require additional treatment to remove the impurities prior to use in future applications.

Compared with batch processes, continuous processes offer many advantages such as a high production rate, consistent quality, and the ability to typically produce spherical and agglomerate-free particles. Recently, spray pyrolysis (SP), a continuous process, has been actively investigated for the preparation of $BaTiO_3$ particles. Furthermore, this process can be further classified into conventional,[15–17] combustion,[18] citric-acid-assisted,[19] salt-assisted,[20] low-pressure[21] and flame-assisted SP (FASP).[22,23] The particles prepared from conventional SP typically have sizes that are submicron in order. Many attempts have been made to reduce the size of prepared $BaTiO_3$ particles to nanosize order. The SP process can be chemically manipulated to produce nanosized $BaTiO_3$ particles by adding CH_6N_4O and NH_4NO_3 (combustion SP),[18] citric acid (CA-SP)[19] or salt (SASP) to the precursor.[20] In low-pressure SP,

* Corresponding author. Tel.: +81 82 424 7716; fax: +81 82 424 5494.
E-mail address: okuyama@hiroshima-u.ac.jp (K. Okuyama).

0955-2219/$ – see front matter © 2007 Elsevier Ltd. All rights reserved.
doi:10.1016/j.jeurceramsoc.2007.04.009

the high drying rate is believed to be the main factor causing fragmentation of $BaTiO_3$ particles to produce nanoparticles.[21]

Among the SP processes, FASP is an attractive method because it is a one-step process that produces various materials of nanosize order. However, there are no published studies demonstrating the preparation of nanosized $BaTiO_3$ particles using FASP. Brewster et al. (1997)[22] reported the production of submicron to micron-sized $BaTiO_3$ particles from a solution of barium acetate and titanium lactate. By the emulsion combustion method, a modified-FASP method, Tani et al. (2001)[23] prepared spherical $BaTiO_3$ particles with a size of about 315 nm. However, the bulk particles were contaminated with Ba_2TiO_4.

In this paper, the preparation of $BaTiO_3$ nanoparticles from aqueous precursor using FASP is described for the first time. The flame process parameters can be manipulated to control the geometric mean diameter and crystal structure of the $BaTiO_3$ particles. The effects of particle size and structure on the dielectric properties of $BaTiO_3$ pellets also are described.

2. Experimental

2.1. Synthesis of $BaTiO_3$

The experimental set-up of the FASP system is shown in Fig. 1. The set-up consisted of an aerosol generator (ultrasonic nebulizer), a diffusion flame reactor and a powder collector. The frequency of the ultrasonic nebulizer transducer was 1.7 MHz. The powder collector was a bag filter, and a vacuum pump was used to transport the particles to the bag filter. A condenser with a water-cooling system was used to condense the water vapor produced during evaporation of the solvents.

The precursor solution was made from $Ba(CH_3COO)_2$ (99%) and titanium-tetra-isopropoxite (TTIP-97%) that had been purchased from Kanto Chemicals (Tokyo, Japan), and used without further purification. One normal HNO_3 was used as the solvent in the precursor preparation. The total concentration of precursor was varied from 0.1 to 0.4 M with a molar ratio of Ba:Ti of 1:1. To produce a clear solution of TTIP, about 50 mL of 1N HNO_3 was added to the TTIP. The mixture was vigorously stirred for about 1 h to ensure thorough mixing of the TTIP and HNO_3. After the clear solution was prepared, predetermined amounts of barium acetate and water were added to the desired volume (100 mL). To ensure homogeneity of the solution, gentle agitation of the final solution was continued for about 1 h.

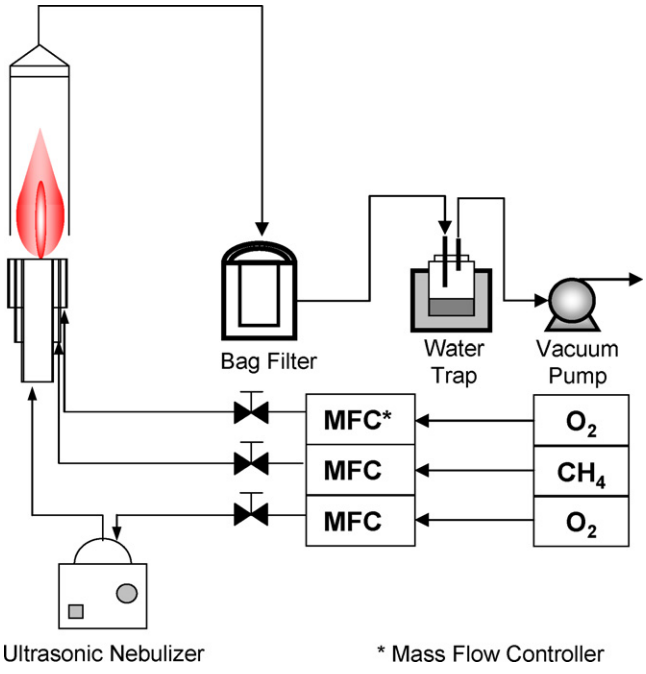

Fig. 1. Experimental set-up of flame assisted spray pyrolysis (FASP).

The experiment was carried out by first atomizing the precursor using an ultrasonic nebulizer to produce droplets. The average droplet size was 5.45 μm, measured using a droplet-size analyzer (Malvern Spraytec, Malvern Instruments Ltd., Worcestershire, United Kingdom). These droplets were transported to the flame zone using oxygen as the carrier gas with a flow rate of 4 L/min. The fuel gas was methane and oxygen acted as the oxidant. The methane flow rate was varied from 3 to 6 L/min to investigate the effect of flame temperature on the characteristics of the prepared particles. During the experiment, the ratio of fuel to oxidant was kept constant at 2.1. The excess oxygen was provided to ensure complete combustion of the fuel and to avoid the generation of carbon from the decomposition of unburned fuel. The prepared particles were collected and then characterized.

2.2. Characterization

The morphology of the particles was observed at 20 kV by field-emission scanning electron microscopy (FE-SEM, S-5000, Hitachi Ltd., Tokyo, Japan). Prior to the analysis, particles were ion-sputtered for 30 s (E-1010, Hitachi, Tokyo, Japan). The geometric mean diameter (d_g) and geometric standard deviation (σ_g) were determined from FE-SEM images by sampling about 200 particles. The detailed morphology and electron diffraction of the crystals were examined in detail by transmission electron microscopy (TEM, JEM-2010, JEOL Ltd., Tokyo, Japan) at 300 kV. The crystal structure of the powder was examined using an X-ray diffractometer (XRD, RINT 2200 V, Rigaku-Denki Corp., Tokyo, Japan). The measurement was carried out using nickel-filtered Cu Kα radiation ($\lambda = 0.154$ nm) at 40 kV and 30 mA with a scan step of 0.02° and a scan speed of 4°/min.

To evaluate the organic content, a Fourier transform infrared (FT-IR) spectrophotometer (IRPrestige-21, Shimadzu Corp., Kyoto, Japan) was used. The FT-IR measurement was carried out at room temperature with a resolution of 2 cm^{-1} using the KBr dilution technique. Thermal properties were investigated by thermal gravimetric analysis (TG) and differential thermal analysis (DTA) (TG-DTA 6200, Seiko Instruments Inc., Tokyo, Japan). TG-DTA was carried out by placing a sample of about 10 mg in a platinum pan, which was then inserted into the analysis chamber. The temperature ranged from 30 to 1000 °C with a heating rate of 10 °C/min under air at a flow rate of 200 mL/min.

The dielectric properties of the product were evaluated using pelleted-$BaTiO_3$. To prepare the pellets, $BaTiO_3$ powder was pressed uniaxially at 10 MPa. The pellets (12 mm in diameter and 1 mm in thickness) were sintered at 1250 °C for 10 h with

a heating rate of 5 °C/min. Electrodes were formed by placing silver paste onto the pellet surface and then heating the pellets in a furnace at a temperature of 500 °C for about 1 h. An individual pellet was placed in a sample holder jig, which was connected to a dielectric interface (Solartron 1296A), and the impedance analyzed (Solartron 1260A, Solartron Analytical, Hampshire, United Kingdom). The dielectric properties were measured at room temperature in the frequency range from 1 kHz to 1 MHz at an ac amplitude of 1 V rms.

3. Results and discussion

3.1. Reaction mechanism of $BaTiO_3$

The knowledge of the reaction mechanism of $BaTiO_3$ under heat treatment will be very useful for explaining the $BaTiO_3$ formation in the flame reactor. TG-DTA analysis gives information about how the precursor responds to heat treatment. The TG-DTA analysis of 0.2 M precursor solution with a ratio of Ba:Ti of 1:1 in the temperature range from 30 to 1000 °C is shown in Fig. 2. The thermal analysis of the precursor in the temperature range from 30 to 150 °C is shown in Fig. 2a. The weight of the sample was reduced to 5.49% of its initial weight when the solution was heated to 88.79 °C. The weight loss of the sample in this temperature region is mainly caused by the evaporation of the solvent. The presence of 50% v 1N HNO_3 in the precursor reduced the boiling point of the solvent to below 100 °C (the boiling point of pure HNO_3 is 83 °C).

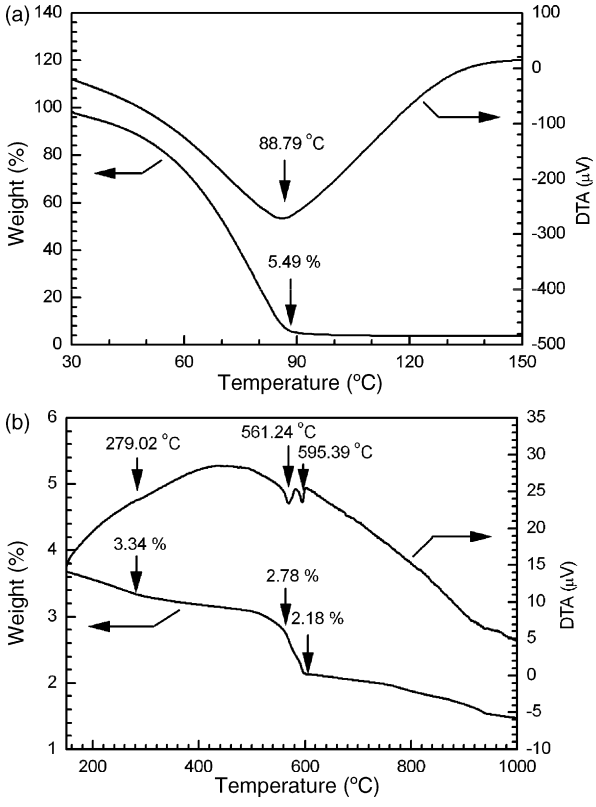

Fig. 2. TG-DTA graph of precursors in the temperature range of 30–150 °C (a) and 150–1000 °C (b).

Fig. 2b shows the TG-DTA plot of the precursor in the temperature range from 150 to 1000 °C. TTIP decomposed into TiO_2 at a temperature of 279.02 °C, and the weight of the remaining sample was reduced to 3.34%. At a temperature of 561.24 °C, $Ba(CH_3COO)_2$ decomposed into $BaCO_3$, and the weight of the remaining sample was 2.78% of the original sample. This result is in agreement with that previously reported by Wang et al.(2005)[21]: TTIP and $Ba(CH_3COO)_2$ decomposed into TiO_2 and $Ba(CO3)_2$ at approximately 250 and 500 °C, respectively. A reaction of $BaTiO_3$ at 595.35 °C was indicated by the decrease in the sample weight to 2.18% of the initial weight. In the above scheme, the formation of $BaTiO_3$ was considered to be a solid-state reaction of $BaCO_3$ and TiO_2.

The formation of $BaTiO_3$ through a solid-state reaction starts from the reaction of $BaCO_3$ and TiO_2.[5–8]

$$TiO_2 + BaCO_3 \rightarrow BaTiO_3 + CO_2$$

The formation of $BaTiO_3$ is accompanied by the release of CO_2 gas as a by-product. The rate of the reaction between $BaCO_3$ and TiO_2 depends strongly on the particle size, the state of aggregation, the degree of mixing and the atmosphere of the reaction. The reaction progresses from the surface of the TiO_2 particles and is controlled by the diffusion of barium ions into the core of the initial TiO_2 particles. The final shape of $BaTiO_3$ particles is the same as the shape of the initial TiO_2 particles, and the particle volume increases by about 27% of the initial volume.[5,6] If the initial size of TiO_2 particles is less than 200 nm, the reaction rate is very fast and the formation of intermediate phases is suppressed.[6,7]

3.2. Control of particle size and morphology

It is important to be able to control the size of the nanoscale $BaTiO_3$ particles. Fig. 3 shows SEM images of particles prepared using different precursor concentrations. In this case, the flame was generated using a methane flow rate of 4 L/min with a carrier gas (oxygen) flow rate of 4 L/min. The precursor concentration was varied from 0.1 to 0.4 M. The geometric mean diameters were 23, 33, 52 and 71 nm for particles prepared from precursor concentrations of 0.1, 0.2, 0.3 and 0.4 M, respectively. Moreover, the geometric standard deviation of particles ranged from 1.28 to 3.15. The increase in particle diameter with increasing precursor concentration is in agreement with a previous study of the production of nanomaterials using a flame process.[24]

In FASP, when a droplet was delivered into the flame zone, evaporation of the solvent occurred. Due to evaporation of the solvent, the droplet concentration increased until the solubility of the solute in the solvent was exceeded. The solution reached supersaturation, leading to precipitation of the solute. At high concentrations, precipitation more readily occurred. The precipitated solute had a longer time to grow, leading to the formation of larger particles compared to those that were produced using low concentration precursor solutions. From TG-DTA analysis, TTIP and $Ba(CH_3COO)_2$ decomposed into TiO_2 and $BaCO_3$ at 279.02 and 561.24 °C, respectively. Thus, after decomposition, the TiO_2 particles produced from high concentration precursor solutions were large in size. Because the size and shape of

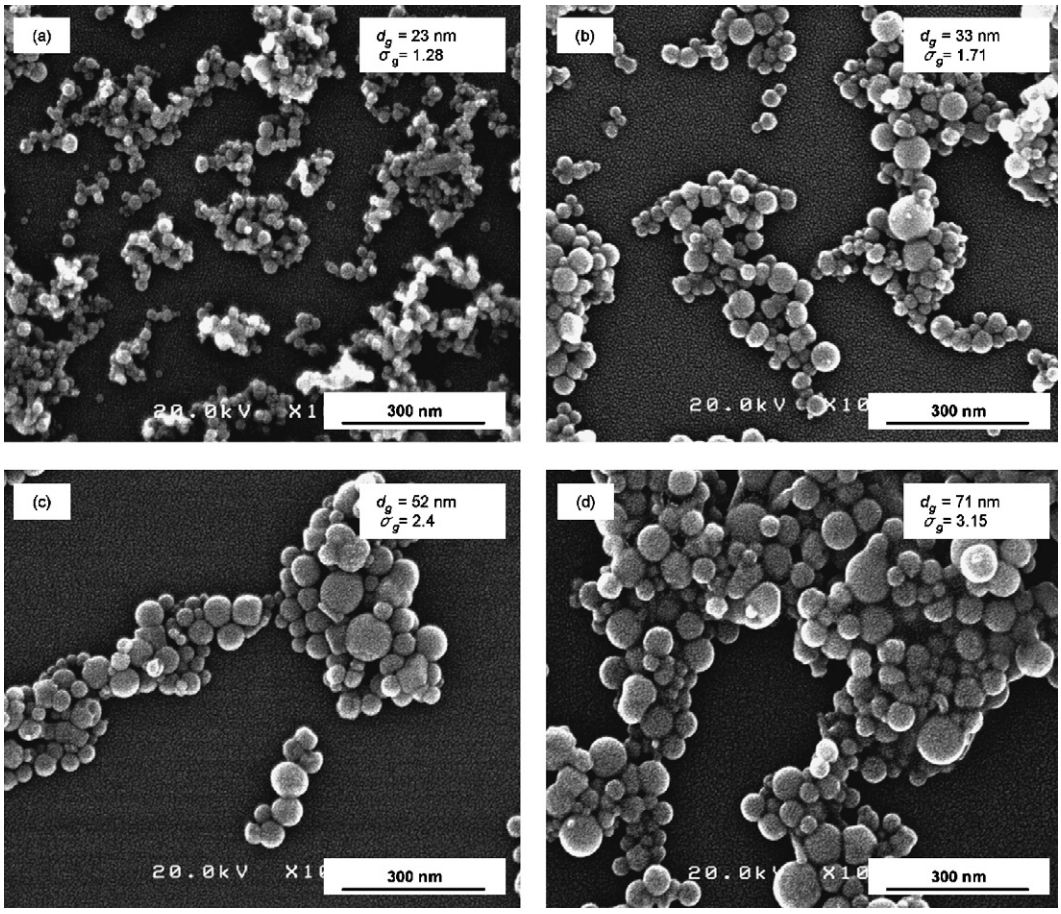

Fig. 3. FE-SEM images of $BaTiO_3$ prepared from precursor concentrations of 0.1 (a), 0.2 (b), 0.3 (c) and 0.4 M (d).

prepared $BaTiO_3$ is highly dependent on the size and shape of the initial TiO_2 particles, the $BaTiO_3$ particles prepared from high concentration precursor solutions also were expected to be large in size.

The size of the particles also was controlled by changing the methane flow rate. As shown previously, altering the methane flow rate changed the flame temperature.[25] Fig. 4 shows SEM images and size distributions of particles as a function of the methane flow rate. The geometric mean diameters of the particles were 33, 33, 37 and 45 nm for methane flow rates of 3, 4, 5 and 6 L/min, respectively. The increase in $BaTiO_3$ particle size with increasing temperature was in agreement with previous results.[20,26] The increased particle size resulted from the high crystal growth rate of particles in the high-temperature environment. Fig. 4 shows that the geometric standard deviation of particles ranged from 1.42 to 1.71. This indicated that tuning of particle size by varying the methane flow rate produced a narrower size distribution than the size range that resulted from altering the precursor concentration.

The $BaTiO_3$ particles prepared from the flame process were spherical with a smooth surface. Changing the precursor concentration did not significantly change particle morphology. However, when a high methane flowrate was applied, a small amount (about 5–10%) of nanorod-like particles were produced (Fig. 4d). The formation of nanorod-like particles was evident in the high magnification image as shown in Fig. 4e (indicated by arrow). Moreover, spherical particles were produced using methane flow rates of up to 5 L/min.

Fig. 5a shows TEM images of particles that were prepared using a methane flow rate of 4 L/min and a precursor concentration of 0.1 M. The as-prepared particles were dense and soft-aggregated with particle size varying from 15 to 40 nm. Analysis of the ring pattern from the selected-area electron diffraction (SAED) confirmed that the material had a cubic structure (Fig. 5a inset). Detected by high-resolution TEM (HRTEM) imaging (Fig. 5b), the cubic $BaTiO_3$ particles had an interplanar spacing of 2.78 Å which corresponded with a crystal orientation of (1 1 0).

3.3. Crystal structure of particles

Fig. 6 shows the XRD patterns of $BaTiO_3$ particles prepared using different concentrations. There was no significant difference in the characteristic peaks among particles produced from different precursor concentrations. The particle structure was cubic-consistent with JCPDS Reference No. 31-0174. From the XRD spectra (Fig. 6), the intensity of the particles slightly increased as the precursor concentration increased. The increase in intensity of the XRD spectra implied the reduction of full width at high maximum (FWHM), indicating the formation of larger crystallite particles.

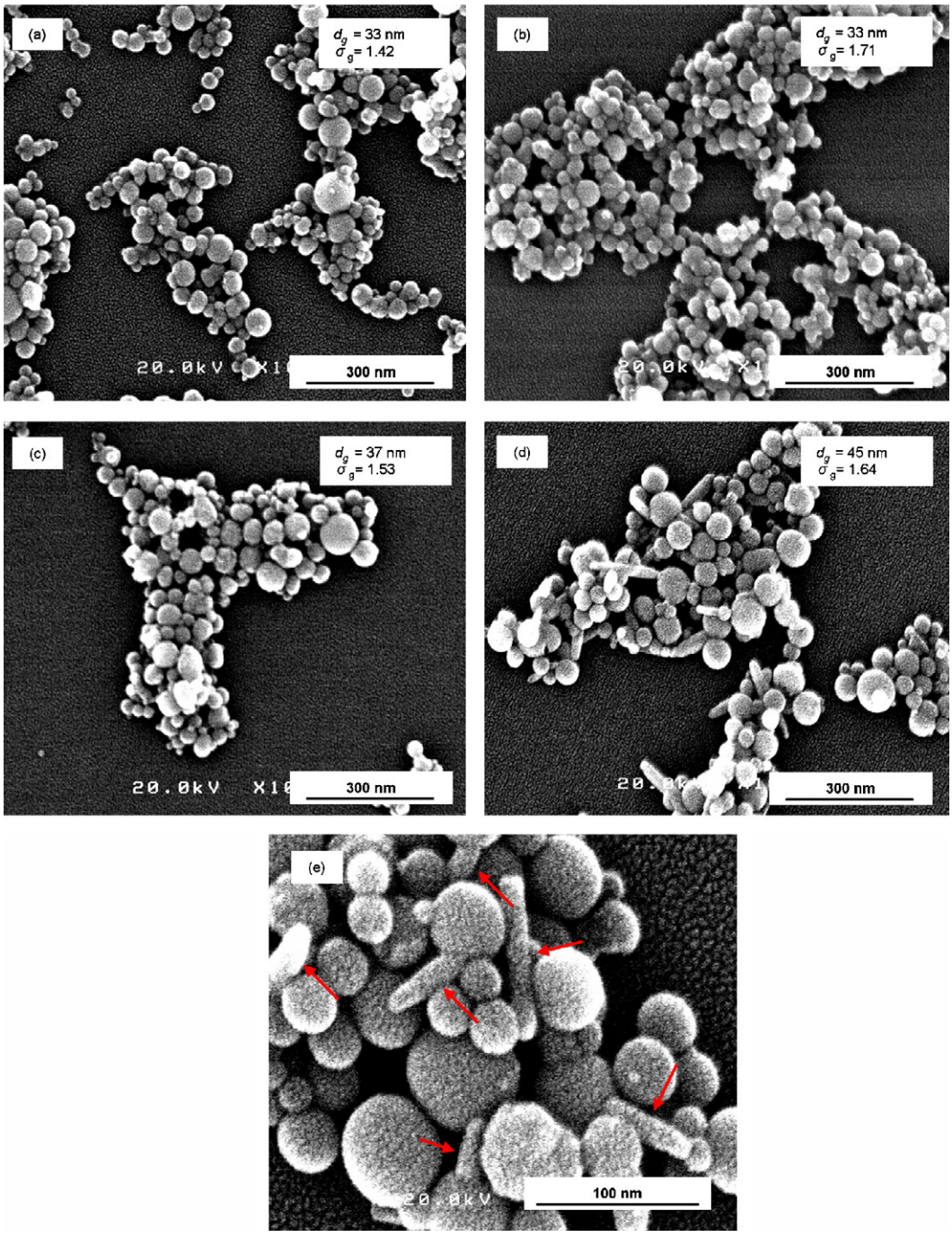

Fig. 4. FE-SEM images of $BaTiO_3$ prepared using methane flow rates of 3 (a), 4 (b), 5 (c) and 6 L/min (d). FE-SEM image at high magnification of particles prepared from methane flow rate 6 L/min (e).

The effect of methane flow rate on particle crystallinity is shown in Fig. 7. Particles prepared using a methane flow rate of 3 L/min showed peaks characteristic of $BaCO_3$ and TiO_2 anatase, in addition to $BaTiO_3$ peaks. These impurities were generated from the uncomplete reaction of $BaCO_3$ and TiO_2 during $BaTiO_3$ formation. Pure $BaTiO_3$ particles were prepared using a methane flow rate of 4 L/min. Another phase structure of $BaTiO_3$ was recognized when methane flow rates of 5 and 6 L/min were applied. These peaks belonged to hexagonal-structure $BaTiO_3$ particles. The formation of the hexagonal phase was due to the high temperature used in the flame process. These results were in agreement with Brewster et al. (1997): prepared particles were also in the hexagonal phase when a high flame temperature was applied.[22] The phase transition of $BaTiO_3$ particles structure was thermal- and size-dependent. The dependency of $BaTiO_3$ phase on the size was indicated by the presence of a critical size. Experimentally, the critical size (transition from cubic to tetragonal phase) was reported at 30 to 190 nm.[27,28] In spray pyrolysis, the transition from cubic to tetragonal phase can be initiated by increasing the furnace temperature.[19]

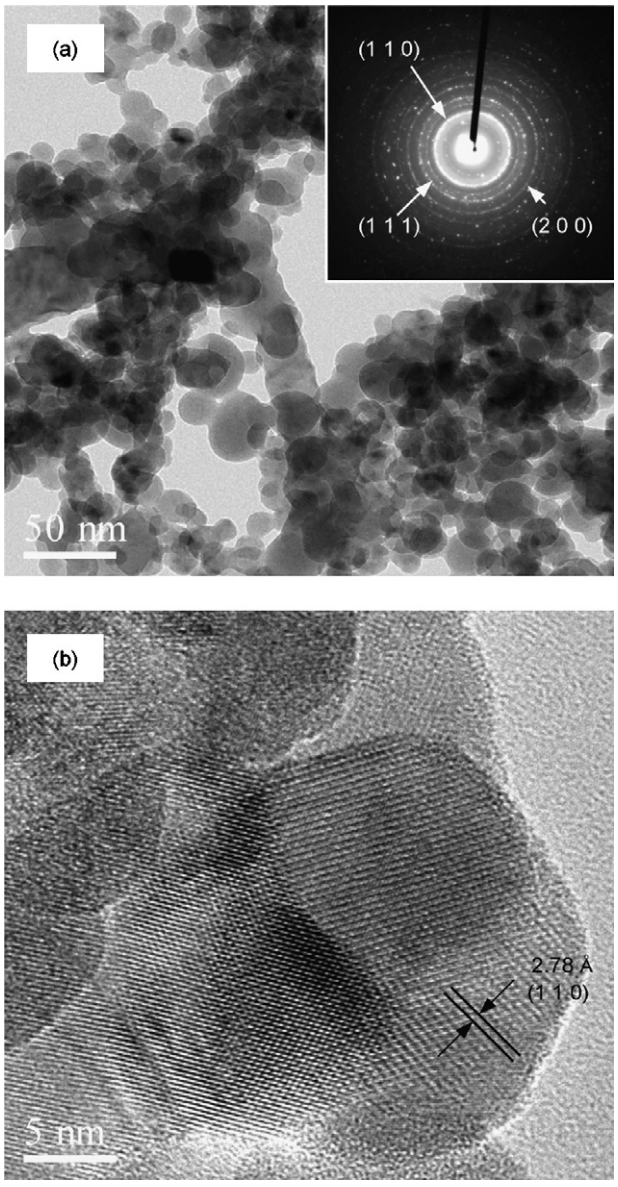

Fig. 5. TEM image (a), electron diffraction pattern (inset in a) and HRTEM image (b) of $BaTiO_3$ powder prepared using a precursor concentration of 0.1 M.

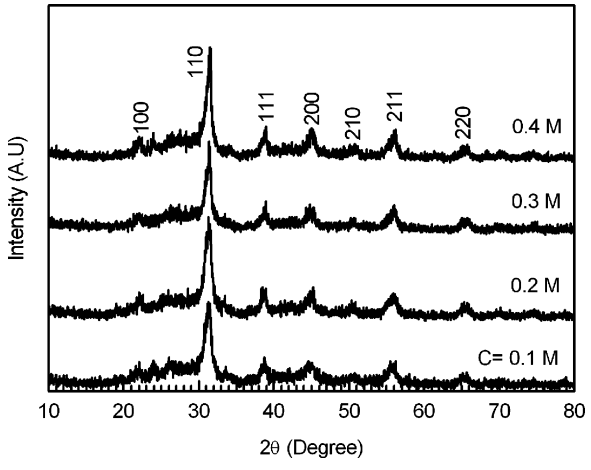

Fig. 6. XRD patterns of $BaTiO_3$ powder prepared from different precursor concentrations.

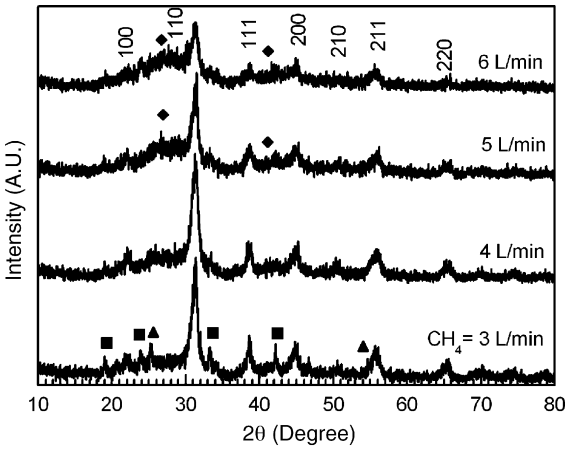

Fig. 7. XRD patterns of $BaTiO_3$ powder prepared using different methane flow rates. ■, $BaCo_3$; ♦, hexagonal $BaTiO_3$; ▲, TiO_2 anatase.

3.4. Organic content of particles

To quantify the organic content of the prepared particles, FT-IR and TG-DTA analysis were carried out. Fig. 8 shows the results of FT-IR analysis of particles prepared using different methane flow rates. The as-prepared particles exhibited three main peaks, corresponding to the bonding vibrations of OH (3420 cm^{-1}),[3] CO_2 (2361 cm^{-1})[12] and carboxyl groups (1417 cm^{-1}).[3] The presence of the –OH bond indicated that as-prepared particles adsorbed water molecules and residual hydroxyl groups.[3] The carboxyl bonding may have originated from unreacted reaction intermediate–$BaCO_3$. The hydroxyl and carboxyl groups were typical impurities of $BaTiO_3$ produced during spray coprecipitation,[3] microwave heating[29] and RF-plasma CVD.[26] The additional organic impurity associated with the FASP-produced $BaTiO_3$ particles was CO_2. In FASP, CO_2 and H_2O were released as products of the combustion process of CH_4. The high concentration of CO_2 in the ambient environment of the $BaTiO_3$ particles caused adsorption of this gas into the particles.

Organic bonding in bulk particles can theoretically be removed by heat treatment. Prior to heat treatment, thermal

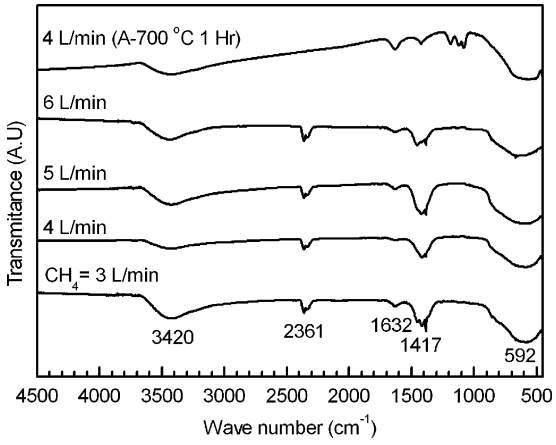

Fig. 8. FT-IR spectra of $BaTiO_3$ powder prepared using different methane flow rates.

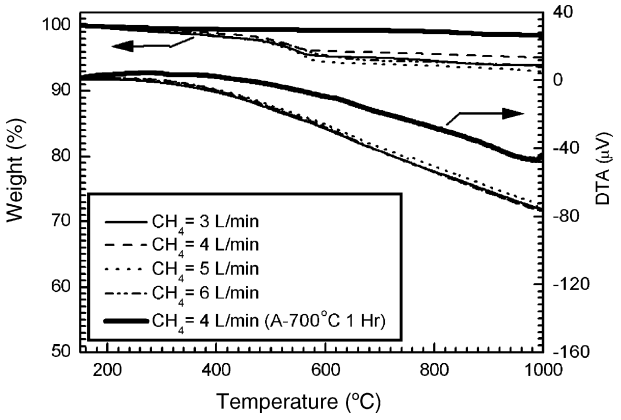

Fig. 9. TGA-DTA spectra of $BaTiO_3$ powder prepared using different methane flow rates.

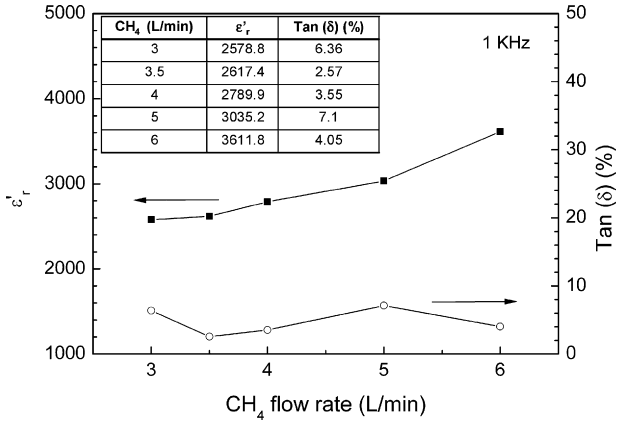

Fig. 10. Dielectric constant and loss factor ($\tan\delta$) of pellets prepared from $BaTiO_3$ powder that had been fabricated using different methane flow rates, measured at room temperature.

analysis was needed to understand the thermal behavior of the particles. Fig. 9 shows the TG-DTA analysis of as-prepared particles at temperatures of up to 1000 °C. Based on TG analysis, it was predicted that organic bonding would decrease in the temperature range of 500–700 °C. The weight loss in the temperature range of 200–400 °C originated from the release of chemisorbed water and hydroxyl groups.[10] At higher temperatures the sample weight decreased slowly and retained 93.88–94.99% of the initial sample weight. Weight loss in this temperature range was attributed to decomposition of carbonate groups into CO_2 gas.[10]

To investigate the removal of organic bonding in the particles by heating, annealing treatment was carried out. The particles were annealed in an electric furnace under air at 700 °C for 1 h with a heating rate of 10 °C/min. The heat-treated particles were then examined by FT-IR and TG-DTA. From the FT-IR analysis, it was concluded that annealing treatment effectively removed

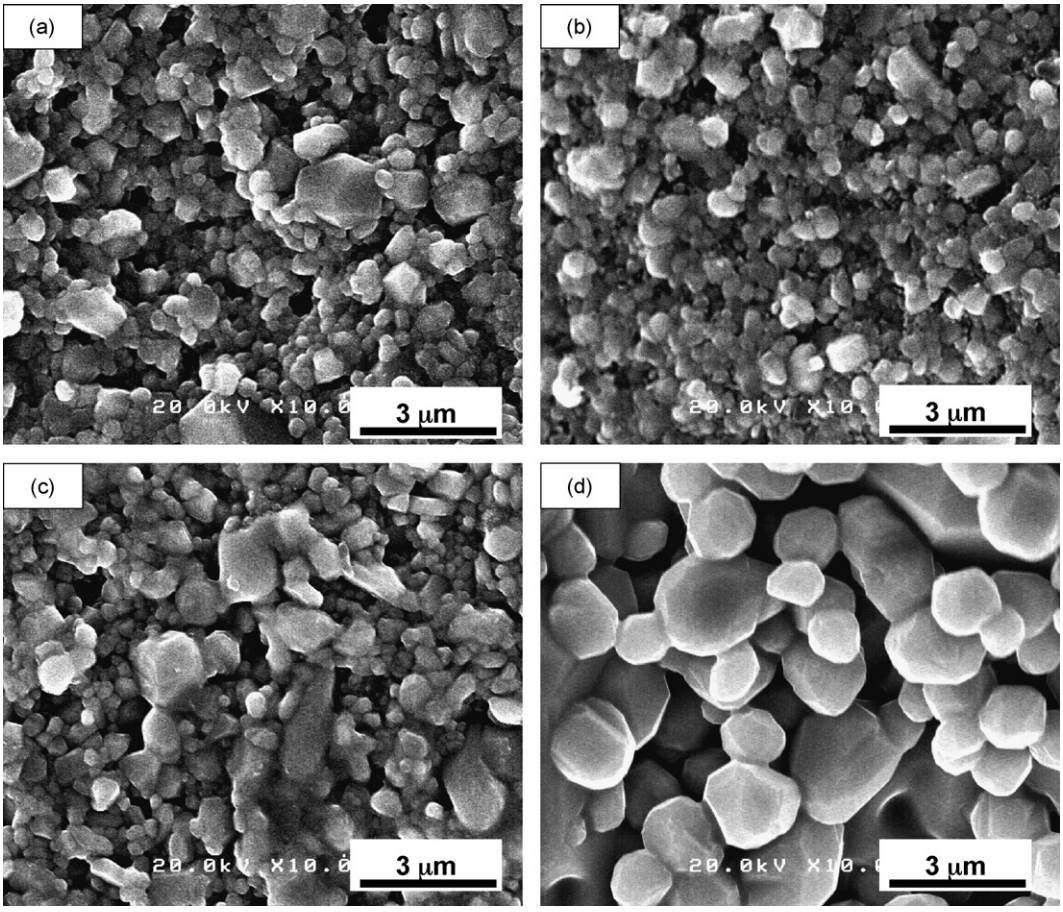

Fig. 11. FE-SEM images of pellet microstructure of the particles prepared from methane flow rates 3 (a), 4 (b), 5 (c) and 6 (d).

organic impurities—CO_2 and carbonate, as shown in Fig. 8. This result was supported by TG analysis (Fig. 9), which showed a small weight loss of 1.67% during heat treatment at temperatures up to 1000 °C.

3.5. Dielectric properties of particles

The dielectric constant and loss factor (tan δ) as a function of methane flow rate is shown in Fig. 10. Dielectric properties were measured at room temperature under bias voltage of 1 V ac at a frequency of 1 KHz. The pellets prepared using particles that were produced at high temperatures (high methane flow rate) tended to have high dielectric constants. The dielectric constants of the $BaTiO_3$ pellets were 2578.8, 2617.4, 2789.9, 3035.2 and 3611.8 for the methane flow rates of 3, 3.5, 4, 5 and 6 L/min, respectively. The loss factor of the corresponding pellets was in the range of 2.57–7.2%.

Measurement of the dielectric properties discussed above was conducted for pellets with the same relative densities (measured by Archimedes' method), ranging from 0.88 to 0.89 of the theoretical $BaTiO_3$ value (6017 kg/m^3). The pellets were sintered at 1250 °C for 10 h with a heating rate of 5 °C/min. The larger $BaTiO_3$ particles tended to produce pellets with larger grain sizes, as shown in Fig. 11. Combined with Fig. 10, there results demonstrated that pellets with large grain size tended to have high dielectric constants. These results were consistent with previous studies in which the size of the initial powder was positively associated with high-dielectric constants of the resulting pellets.[1,2] In summary, since FASP-produced $BaTiO_3$ particles had relatively high dielectric constants, these particles would be suitable for MLCC fabrication.

4. Conclusions

FASP synthesis of $BaTiO_3$ nanoparticles permitted effective control of particle size. Increasing the precursor concentration from 0.1 to 0.4 M produced $BaTiO_3$ particles with diameters in the range of 23–71 nm. Moreover, controlling the flame temperature, by increasing the methane flow rate from 3 to 6 L/min, produced powders with geometric mean diameters ranging from 33 to 45 nm. Generally, the particles produced were spherical, dense, highly crystalline and soft-aggregated. The crystal structure of $BaTiO_3$ was strongly determined by the flame temperature: a low flame temperature produced $BaTiO_3$ particles with impurities, i.e., $BaCO_3$ and TiO_2, due to uncomplete reactions. The structure of $BaTiO_3$ nanoparticles was cubic, and a hexagonal phase was formed when high methane flow rates, i.e., 5 and 6 L/min, were applied. The FASP-produced $BaTiO_3$ particles contained OH, carboxyl and CO_2 in their matrices. However, the organic bonding was completely removed by heat treatment in a furnace at 700 °C for 1 h. The dielectric constants of $BaTiO_3$ pellets ranged from 2578.8 to 3611.8 with loss factors ranging from 2.46% to 7.2%. These results show that FASP is a promising method for producing $BaTiO_3$ nanoparticles with good electrical properties.

Acknowledgements

The authors wish to thank the Ministry of Education, Culture, Sports, Science and Technology of Japan for providing a doctoral scholarship (A.P), a JSPS (Japan Society for the Promotion of Science) post-doctoral fellowship (W.N.W) and a grant-in-aid (K.O, I.W.L). In addition, the authors thank Prof. T. Iizawa for providing the FT-IR analysis equipment, Mr. T. Ogi for the TEM analysis and Mr. T. Ozaki for assistance with the experiment.

References

1. Zhao, Z., Buscaglia, V., Viviani, M., Buscaglia, M. T., Mitoseriu, L., Testino, A. *et al.*, Grain-size effects on the ferroelectric behavior of dense nanocrystalline $BaTiO_3$ ceramics. *Phys. Rev. B: Condens. Matter.*, 2004, **70**, 024107.
2. Caruntu, G., Rarig Jr., R., Dumitru, I. and O'Connor, C. J., Annealing effects on the crystallite size and dielectric properties of ultrafine $Ba_{1-x}Sr_xTiO_3$ powders synthesized through an oxalate-complex precursor. *J. Mater. Chem.*, 2005, **16**, 752–758.
3. Choi, G. J., Lee, S. K., Woo, K. J., Koo, K. K. and Cho, Y. S., Characteristics of $BaTiO_3$ particles prepared by spray-coprecipitation method using titanium acylate-based precursors. *Chem. Mater.*, 1998, **10**, 4104–4113.
4. Clark, I. J., Takeuchi, T., Ohtori, N. and Sinclair, D. C., Hydrothermal synthesis and characterisation of $BaTiO_3$ fine powder: precursor, polymorphism and properties. *J. Mater. Chem.*, 1999, **9**, 83–91.
5. Buscaglia, M. T., Bassoli, M. and Buscaglia, V., Solid-state synthesis of ultrafine $BaTiO_3$ powders from nanocrystalline $BaCO_3$ and TiO_2. *J. Am. Ceram. Soc.*, 2005, **88**, 2374–2379.
6. Amin, A., Spears, M. A. and Kulwicki, B. M., Reaction of anatase and rutile with barium carbonate. *J. Am. Ceram. Soc.*, 1983, **66**, 733–738.
7. Hennings, D. F. K., Schrenemacher, B. S. and Schrenemacher, H., Solid-state preparation of $BaTiO_3$-based dielectrics, using ultrafine raw materials. *J. Am. Ceram. Soc.*, 2001, **84**, 2777–2782.
8. Beauger, A., Mutin, J. C. and Niepce, J. C., Synthesis reaction of metatitanate $BaTiO_3$. Part 1. Effect of gaseous atmosphere upon the thermal evolution of the system $BaCO_3$–TiO_2. *J. Am. Ceram. Soc.*, 1983, **18**, 3041–3046.
9. Testino, A., Buscaglia, V., Buscaglia, M. T., Viviani, M. and Nanni, P., Kinetic modeling of aqueous and hydrothermal synthesis of barium titanate ($BaTiO_3$). *Chem. Mater.*, 2005, **17**, 5346–5356.
10. Boulos, M., Guillemet-Fritsch, S., Mathieu, F., Durand, B., Lebey, T. and Bley, V., Hydrothermal synthesis of nanosized $BaTiO_3$ powders and dielectric properties of corresponding ceramics. *Solid State Ionics*, 2005, **176**, 1301–1309.
11. Maso, N., Beltran, H., Cordoncillo, E., Flores, A. A., Escribano, P., Sinclair, D. C. *et al.*, Synthesis and electrical properties of Nb-doped $BaTiO_3$. *J. Mater. Chem.*, 2006, **16**, 3114–3119.
12. Mullens, J., Van Werde, K., Vanhoyland, G., Nouwen, R., Van Bael, M. K. and Van Poucke, L. C., The use of TGA-MS, TGA-FTIR, HT-XRD and HT-DRIFT for the preparation and characterization of $PbTiO_3$ and $BaTiO_3$. *Thermochim. Acta.*, 2002, **392**, 29–35.
13. Testino, A., Buscaglia, M. T., Viviani, M., Buscaglia, V. and Nanni, P., Synthesis of $BaTiO_3$ particles with tailored size by precipitation from aqueous solutions. *J. Am. Ceram. Soc.*, 2004, **87**, 79–83.
14. Anuradha, T. V., Ranganathan, S., Mimani, T. and Patil, K. C., Combustion synthesis of nanostructured barium titanate. *Scr. Mater.*, 2001, **44**, 2237–2241.
15. Nonaka, K., Hayashi, S., Okada, K. and Otsuka, N., Characterization and control of phase segretion in the fine particles of $BaTiO_3$ and $SrTiO_3$ synthesized by the spray pyrolysis method. *J. Mater. Res.*, 1991, **6**, 1750–1756.
16. Milosevic, O. B., Mirkovic, M. K. and Uskokovic, D. P., Characteristics and formation mechanism of $BaTiO_3$ Powders prepared by twin-fluid and ultrasonic spray-pyrolysis methods. *J. Am. Ceram. Soc.*, 1996, **79**, 1720–1722.
17. Guo, W., Datye, A. K. and Ward, T. L., Synthesis of barium titanate powders by aerosol pyrolysis of a Pechini-type precursor solution. *J. Mater. Chem.*, 2005, **15**, 470–477.

18. Lee, S., Son, T., Yun, J., Kwon, H., Messing, G. L. and Jun, B., Preparation of $BaTiO_3$ nanoparticles by combustion spray pyrolysis. *Mater. Lett.*, 2004, **58**, 2932–2936.
19. Lee, K. K., Kang, Y. C., Jung, K. Y. and Kim, J. H., Preparation of nano-sized $BaTiO_3$ particle by citric acid-assisted spray pyrolysis. *J. Alloys Compd.*, 2005, **395**, 280–285.
20. Itoh, Y., Lenggoro, I. W., Okuyama, K., Madler, L. and Pratsinis, S. E., Size tunable synthesis of highly crystalline $BaTiO_3$ nanoparticles using salt-assisted spray pyrolysis. *J. Nanopart. Res.*, 2003, **5**, 191–198.
21. Wang, W. N., Lenggoro, I. W., Terashi, Y., Wang, Y. C. and Okuyama, K., Direct synthesis of barium titanate nanoparticles via a low pressure spray pyrolysis method. *J. Mater. Res.*, 2005, **20**, 2873–2882.
22. Brewster, J. H. and Kodas, T. T., Generation of unagglomerated, dense, $BaTiO_3$ particles by flame-spray pyrolysis. *AIChE J.*, 1997, **43**, 2665–2669.
23. Tani, T., Takatori, K. and Watanabe, N., Characteristics and sintering behaviour of barium titanate powder synthesized by emulsion combustion method. *J. Ceram. Soc. Jpn.*, 2001, **119**, 981–985.
24. Pratsinis, S. E., Flame aerosol synthesis of ceramic powders. *Prog. Energy. Combust. Sci.*, 1998, **24**, 197–219.
25. Purwanto, A., Wang, W. N., Lenggoro, I. W. and Okuyama, K., Formation and luminescence enhancement of agglomerate-free YAG:Ce^{3+} submicron particles by flame-assisted spray pyrolysis. *J. Electrochem. Soc.*, 2007, **154**, J91–J96.
26. Suzuki, K. and Kijima, K., Phase transformation of $BaTiO_3$ nanoparticles synthesized by RF-plasma CVD. *J. Alloys Compd.*, 2006, **419**, 234–242.
27. Hoshina, T., Kakemoto, H., Tsurumi, T., Wada, S. and Yashima, M., Size and temperature induced phase transition behaviors of barium titanate nanoparticles. *J. Appl. Phys.*, 2006, **99**, 054311–54318.
28. Begg, B. D., Vance, E. R. and Nowotny, J., Effect of particle size on the room-temperature crystal structure of barium titanate. *J. Am. Ceram. Soc.*, 1994, **77**, 3186–3192.
29. Ma, Y., Vileno, E., Suib, S. L. and Dutta, P. K., Synthesis of tetragonal $BaTiO_3$ by microwave heating and conventional heating. *Chem. Mater.*, 1997, **9**, 3023–3031.